Polarimetric Modeling, Calibration and Active Imaging at 91 GHz

M. Canavero, A. Murk
Institute of Applied Physics
University of Bern
Sidlerstr. 5, CH-3012 Bern, Switzerland
E-mail: marco.canavero@iap.unibe.ch, axel.murk@iap.unibe.ch

***Abstract*- The potential and success of remote sensing heavily depends on the existence of complete understanding of the processes under investigation. This requires advancing the existing models that describe the observed phenomena, improving the accuracy of calibration techniques and investigating and testing new applications for remote sensing. In this paper we present the recent improvements achieved in modeling, calibration techniques and active imaging at 91 GHz with polarimetric imaging radiometer.**

I. SPIRA RADIOMETER

The Scanning Polarimetric Imaging Radiometer (SPIRA) is a fully polarimetric imager in the 90-92 GHz [1]. The instrument can measure simultaneously the 4 Stokes parameters for an observed scene using two orthogonally polarized receiver channels and an analog adding correlation network with 2 GHz of bandwidth. The integration time/pixel is 18 ms while average acquisition time/image and receiver noise temperature are respectively 5 min and 600K.

The antenna consists of a dual polarized corrugated feed horn and a 90°-axis parabolic reflector with an effective focal length of 70cm and a projected aperture of 45cm. The co and cross-polar antenna pattern of the instrument has been simulated using software package GRASP. The simulations result in a full-with-half-maximum beam width of about 0.5, which has been confirmed by far-field antenna measurements with a 91 GHz transmitter.

The scene is scanned in two dimensions: the off-set parabolic reflector is rotated around the horizontal bore-sight axis of the feed horn (elevation), whereas the antenna and the polarimeter support are rotated around the vertical axis (azimuth). In both axes stepping motors, with a gear mechanism and optical encoder for the absolute referencing, are used. Figure 1 gives a schematic overview of the SPIRA polarimeter. It consists of two heterodyne receiver chains, which are both connected to the feed horn through an orthomode transducer (OMT). The OMT has a polarization isolation of more than 30 dB, which corresponds to 3.2% mixing of the co- and the cross-polar signal in the correlator. This effect has to be corrected by the polarimetric calibration of the instrument. In each channel an additional noise signal from a switchable noise diode can be injected through a directional coupler, which is used together with an ambient

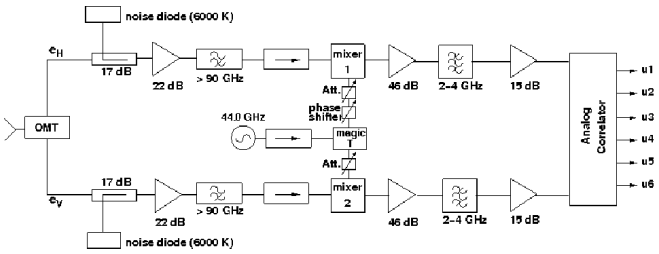

Figure 1: Schematic overview of SPIRA receiver

temperature blackbody calibration target to calibrate the gain and system temperature of the receiver at the end of each antenna scan.

A high pass filter follows the coupler, selecting the upper sideband of the subharmonic Schottky mixers. They are fed by a common local oscillator (44 GHz) to ensure the phase coherence between the two receiver channels. Optimum pumping of the mixers and fine adjustment of the phase shift between the channels are achieved by variable attenuators and a phase shifter in the local oscillator path. The down-converted signals are amplified by low-noise IF amplifiers and band limited to frequencies between 2 and 4 GHz.

For polarimetric observations it is necessary to determine the complex cross-correlation between the two IF signals. For that reason an analog adding correlator is used, which consists of a network of 90° and 180° hybrid couplers followed by six square law detectors and video amplifiers. From the 6 output voltages the four Stokes are reconstructed in the following way:

$$\begin{pmatrix} I \\ Q \\ U \\ V \end{pmatrix} = M \begin{pmatrix} u_6 + u_1 \\ u_6 - u_1 \\ u_5 - u_4 \\ u_3 - u_2 \end{pmatrix} \qquad (1)$$

Where M represents the identity matrix in an ideal polarimeter. In practice however, all couplers have a certain amount of amplitude and phase imbalance. This leads to mixing terms of the different output voltages, which is corrected together with the crosstalk of the OMT by a polarimetric calibration process, represented by the Müller matrix M.

II. RADIOMETRIC MODELING

In our research we are interested in developing models which will predict the Stokes parameters of a given observation. Our models, based on Fresnel equations and Snell law of refraction for layered media, are adapted to a 2-channel receiver capable to determining horizontal and vertical brightness temperature of the scene. First we consider the classical situation for the Fresnel formulas, two half spaces separated by an infinite plane or medium boundary and an incident light ray that strikes at axis origin the interface between the two media of refractive indexes n_1 and n_2., as shown in Figure 2. The angles between the incident, reflected and refracted rays and the normal of the interface are given as θ_i, θ_r and θ_t, respectively. The relationship between these angles is given by the law of reflection:

$$\theta_i = \theta_r = \theta_1 \qquad (2)$$

And Snell's law:

$$\frac{\sin(\theta_i)}{\sin(\theta_t)} = \frac{n_2}{n_1} \qquad (3)$$

In remote sensing applications medium 1 is usually the atmosphere (n_1~1) and n_2 is the refractive index of the surface material. Moreover the values of brightness temperature of a scene are strictly dependent on the reflectivity of each element for vertical and horizontal polarizations.

These considerations lead us to the Fresnel Equation for horizontal (or TM) and vertical (or TE) polarizations, in a not-magnetic media ($n \approx \varepsilon_r$):

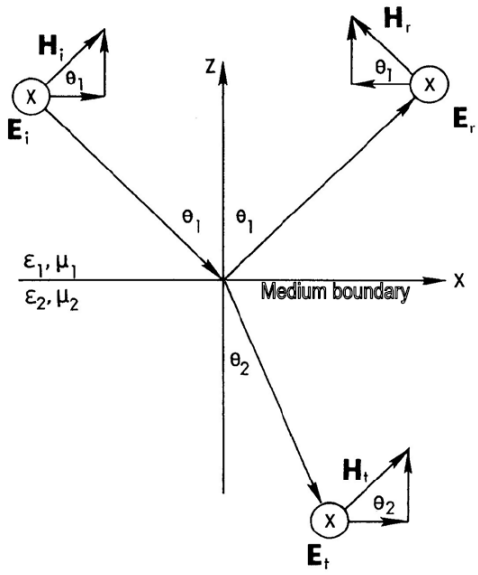

Figure 2: Geometry of horizontal polarized incident, reflected and transmitted waves

$$R_h = \frac{n_1\cos\theta_1 - n_2\cos\theta_2}{n_1\cos\theta_1 + n_2\cos\theta_2}; R_v = \frac{n_2\cos\theta_1 - n_1\cos\theta_2}{n_2\cos\theta_1 + n_1\cos\theta_2} \qquad (4)$$

Then *reflectivity r* and *transmittivity t* for both polarizations are:

$$r_h = |R_h|^2; r_v = |R_v|^2 \qquad (5)$$

$$t_h = 1 + r_h; t_v = 1 + r_v \qquad (6)$$

As mentioned before they are dependent on permittivity of materials. We developed models for different surfaces in order to calculate their permittivity at frequencies of interest.

Once we calculate with our models reflectivity and transmittivity of the selected surface for both polarizations, the relative brightness temperature is the sum of the radiation emitted and the fraction of sky radiation reflected by the surface:

$$T_{pb} = (1 - r_p)T_{amb} + r_p T_{sky} \qquad (7)$$

Where r_p refers to the horizontal or vertical reflectivity, T_{amb} is the ambient (or object) temperature and T_{sky} is the sky temperature. For a plane-parallel atmosphere and under the assumption that the atmosphere is isothermal, T_{sky} depends by the angle of the incoming wave (or *zenith angle*) and the zenith opacity τ_0 and is calculated in our model as:

$$T_{sky} = T_{amb}(1 - \exp(\frac{-\tau_0}{\cos\theta_{sky}})) \qquad (8)$$

Zenith opacity τ_0 can be obtain on-field by SPIRA performing a tipping curve measurement and depends on atmospheric conditions (e.g. clouds, humidity).

From brightness temperature we can finally derive the I and Q Stokes parameter, which can be compared with SPIRA results, as:

$$I = \frac{T_h + T_v}{2} \qquad (9)$$
$$Q = T_h - T_v$$

Some media, like snow, are strongly layered. Then several reflections from different layer interfaces will play a role. A similar problem occurs if the transition between the upper and lower medium is not an abrupt one, but extend over certain distance. Both cases can be handled by general formulas for layered media. The superposition of Fresnel reflection and transmission equations with proper adjustments, in fact, can provide a solution suitable for numerical computation. The reflection and transmission coefficients (R and T) and the derived reflectivity and transmissivity of a multilayer sandwich can be computed by a recursive formula called *invariant*

embedding [2]. Considering an M-layered medium structured as the following figure:

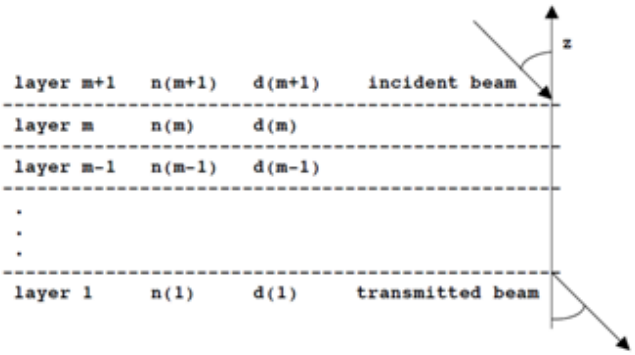

Figure 3: Geometry of layered medium

In which every *m*-layer has a complex refractive index $n_m=n_m'+in_m''$ and a thickness d(m), the bottom medium has number 1 with propagation angle θ_1 to the z-axis, relative permittivity ε_1 and relative permeability μ_1. We call F_1 its Fresnel reflection coefficient and G_1 the transmission coefficient at the boundary from medium 2 (which is the layer of thickness d(2) above medium 1) and medium 1. We define the respective parameters (θ_m, ε_m ...) for each layer and for an incident EM wave (m+1) coming from above our layered medium. The recursive formulas for j=2... M are:

$$R_j = \frac{F_j + R_{(j-1)}Q_j^2}{1+F_jR_{(j-1)}Q_j^2};$$
$$T_j = \frac{G_jR_{(j-1)}Q_j}{1+F_jR_{(j-1)}Q_j^2}; \qquad (10)$$
$$j = 2,3,\ldots,M$$

While for j=1 the values are simply given by: $R_1 = F_1$; $T_1 = G_1$. The factor Q_j describes the complex phase change of the wave on its way through layer j:

$$Q_j = \exp(ik_jd_j\cos\theta_j) \qquad (11)$$

It is important to notice that F_j and G_j depend on polarization. Then also the final reflection and transmission coefficients R and T at the top of the sandwich are different for both polarizations. Reflectivity and Transmissivity are obtained in the same way explained before through the relation (6).

If the surfaces are tilted, in refer to the observation point, the angle of incidence changes, and polarizations on the surface have to be translated in vertical and horizontal polarizations for the observer. For example, in the situation shown in Figure 4, a surface facing the radiometer has a slope of a certain angle β. This means that the local angle of incidence has changed to

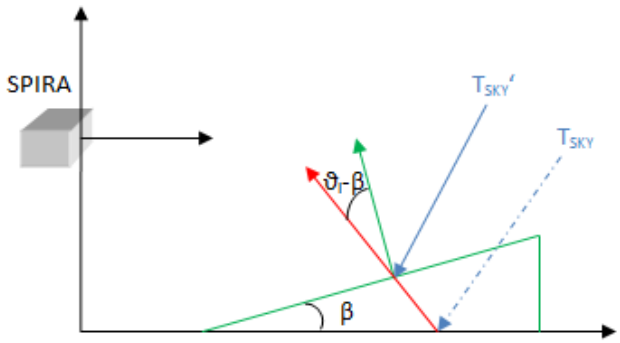

Figure 4: Surface slope in front of the SPIRA radiometer

$\vartheta_{sky}' = \beta - \vartheta_{sky}$. In this case in order to obtain the desired brightness temperatures at SPIRA receiver we have to:

- Calculate reflectivity and transmittivity of the surface (as it is in plain) with given angle ϑ_{sky}, obtaining r_{TM} and r_{TE}.
- Apply the following formulas to obtain the brightness temperatures at SPIRA receiver:

$$\vartheta_{sky}' = \beta - \vartheta_{sky} \qquad (12)$$

$$T_{sky}' = T_{surf}(1-e^{-\frac{\tau_0}{\cos\vartheta_{sky}'}}) \qquad (13)$$

$$T_v = (1-r_{TM})T_{surf} + r_{TM}T_{sky}' \qquad (14)$$

$$T_h = (1-r_{TE})T_{surf} + r_{TE}T_{sky}' \qquad (15)$$

I and Q Stokes can be obtained using (9).

If the surface is rotated by an angle ψ, in relation to the origin of vertical and horizontal axis of the radiometer, we occur in the situation depicted in Figure 5. In this case a U component is present, and as to be taken in account.

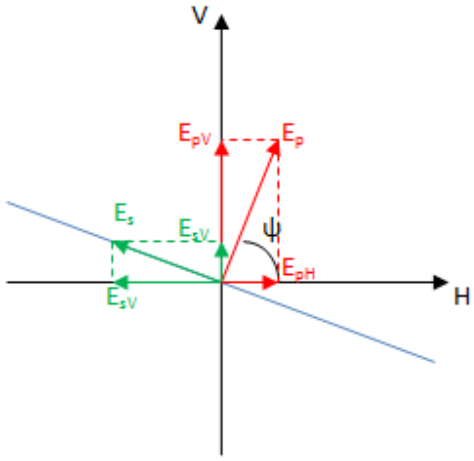

Figure 5: Rotated surface in front of SPIRA radiometer

If we project the intensities of E_p and E_s on the V and H axis and take the difference between these two in order to attain the U parameter, there will only result something unequal to zero if $\psi \neq 0$. The intensities of horizontal, vertical and ± 45° polarization can be expressed as:

$$I_h \propto E_p^{\,2} \cos^2\psi + E_s^{\,2} \sin^2\psi \qquad (16)$$

$$I_v \propto E_p^{\,2} \sin^2\psi + E_s^{\,2} \cos^2\psi \qquad (17)$$

$$I_{+45°} \propto E_p^{\,2} \cos^2(\psi - 45°) + E_s^{\,2} \sin^2(\psi - 45°) \qquad (18)$$

$$I_{-45°} \propto E_p^{\,2} \sin^2(\psi - 45°) + E_s^{\,2} \cos^2(\psi - 45°) \qquad (19)$$

TM and TE brightness temperatures calculated on the surface by Fresnel Equations are directly proportional to E_p and E_s. We can assign:

$$\begin{aligned} A &= (1 - r_{TM})T_{surf} + r_{TM}T_{sky} \propto E_p \\ B &= (1 - r_{TE})T_{surf} + r_{TE}T_{sky} \propto E_s \end{aligned} \qquad (20)$$

Then we can express the brightness temperature measured by SPIRA as:

$$\begin{aligned} &T_v = A\sin\psi + B\cos\psi ; T_h = A\cos\psi + B\sin\psi \\ &I = \frac{T_v + T_h}{2} ; Q = T_v - T_h \end{aligned} \qquad (21)$$

Similarly, for U Stokes:

$$\begin{aligned} U &= [A\cos(\psi - 45°) + B\sin(\psi - 45°)] \\ &-[A\sin(\psi - 45°) + B\cos(\psi - 45°)] = \\ &= (A - B)[\cos(\psi - 45°) - \sin(\psi - 45°)] \end{aligned} \qquad (22)$$

The following figures show some example of computed models [3]. In Figures 6 and 7 an example of I and Q Stokes for different horizontal surfaces, for scan-angles between 0° and 90° is shown. In figure 8 the vertical and horizontal polarizations of a concrete layer, with a slope of 0°, 45° and 90°, are shown. The first tests of model validation look promising and complete results will be published in following papers.

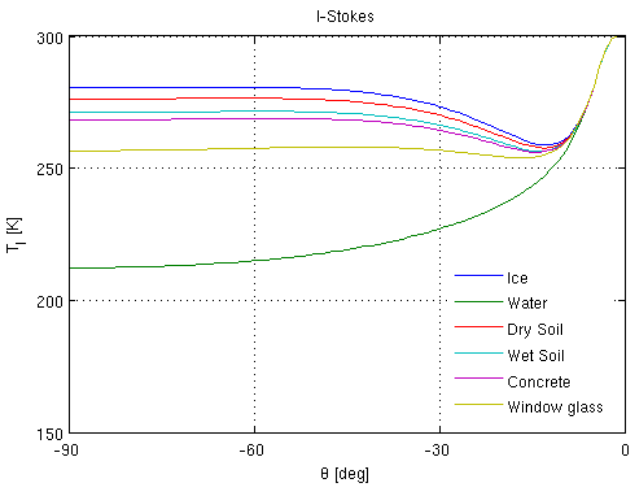

Figure 6: Simulated I Stokes brightness temperatures for different material, horizontal surfaces. T_{surf} = 300K, Zenith opacity at 0.2, f = 91 GHz

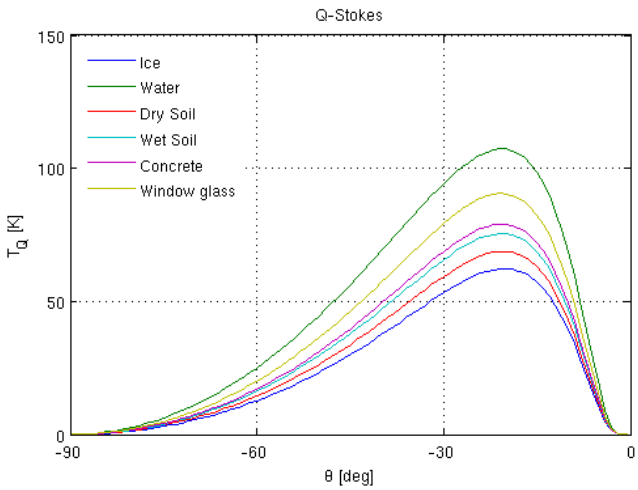

Figure 7: Simulated Q Stokes brightness temperatures for different material, horizontal surfaces. T_{surf} = 300K, Zenith opacity at 0.2, f = 91 GHz

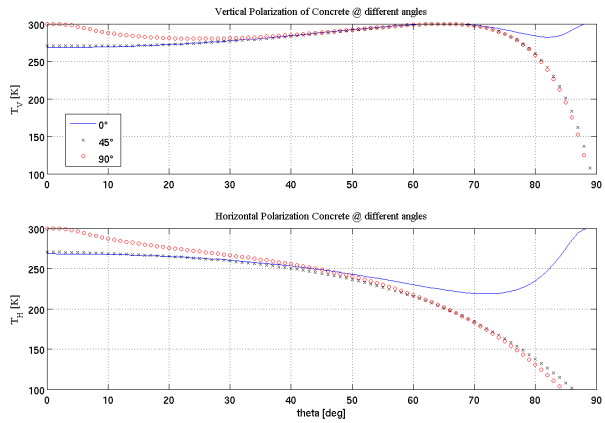

Figure 8: Vertical and horizontal polarization brightness temperature for a layer of concrete with slope β = 0°, 45° and 90°. T_{surf} = 300K, Zenith opacity at 0.2, f = 91 GHz

III. New Polarimetric Calibration Target

In order to obtain the correct Stokes parameters the radiometer must be calibrated for both total power and polarimetry. Polarimetric calibration must take in account the amplitude and phase umbalance of the correlation network and OMT and is achieved with a tailored calibration source that emits signals with different polarizations, in order to obtain the Müller matrix that polarimetrically calibrates the system.

In the past this task was performed using a combination of liquid nitrogen, a retarding plate and a wire grid [4]. This arrangement is impractical on outdoor measuring campaigns

and for this reason we are developing a new polarimetric calibration technique, more suitable for field measures.

The off-set parabolic reflector configuration of the radiometer can be properly used for this purpose. The rotating axis of SPIRA, normally used for elevation scans, can host a horn antenna transmitting a linear polarized signal. It is possible to calibrate the output channels of the receiver and, consequently I, Q and U Stokes parameters, just positioning the polarized signal at different angles.

For the calibration of V Stokes we need a circularly polarized reference signal. This task can be achieved by introducing a retarder between the transmitter and receiver. A retarder introduces a phase shift between two orthogonal polarization components and can be realized in different ways, e.g. by introducing a path length difference by reflection or using materials that have different permittivity in orthogonal directions. The latter can be either physically inserted in the waveguide feeding the transmitting or receiving horn or in between the two horns. The first option requires a septum polarizer, while the second option requires a λ/4-wave-plate retarder, and a schematic overview of this configuration is shown in Figure 9.

If an elliptical polarization is achieved, the rotating axis of SPIRA over 360° can still help to obtain a calibration matrix for V Stokes.

The plate, made by high density polyethylene (HDPE), can be design in a way to minimize the reflections. For characterization and modeling by Müller-matrix reflections, absorption and manufacturing irregularities of the plate must be taken in account. The retarder plate has an important practical advantage in respect to septum polarizer; in fact it can be mounted on a support and hooked in front of the rotating transmitting antenna only when V Stokes parameter is calibrated, while septum in waveguide requires to be disassembled from the feeding horn.

A test prototype of the calibration source was built in our department and measurements with either septum or plate were performed. Both showed good performances at 91 GHz, but for practical reason, mentioned above, the retarder plate has been chosen for our final calibration device. Figure 10 shows the phase shift achieved by retarder plate, between the two orthogonal components of a linear polarized signal.

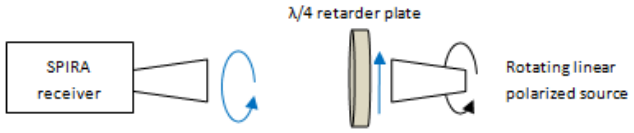

Figure 9: Schematic overview of the calibration device for calibrating V Stokes. A retarder plate is inserted between Tx and Rx, a linear polarized signal is retarder in order to obtain a circularly polarized wave (in blue)

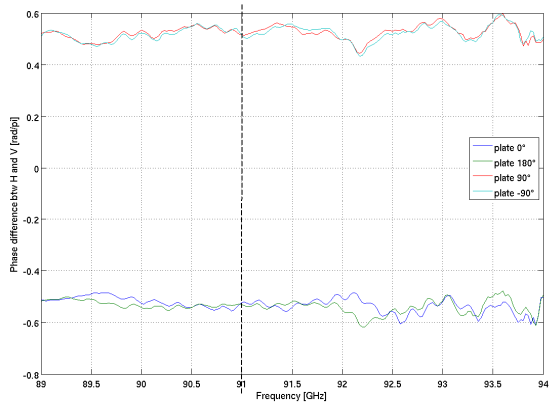

Figure 10: Measured phase difference in radians between horizontal and vertical receiving signals when a linear polarized signal at 45° (referred to the V receiver axis) is transmitted. The retarder plate has an orientation (same reference) of respectively 0°, 90°, 180° and 270°. A phase difference of 0.5 rad origins a circular polarization

IV. Active Measurements

The implementation of an active source for a passive radiometer can, under certain conditions, increment the contrast of the images acquired and add extra information to the measures. It can also turn an essentially outdoor system in an indoor one (compensating with active illumination the absence of cold sky radiation). This topic was investigated by conducting observations of various scenes with SPIRA polarimeter.

First indoor experiments with active illumination by a laboratory CW signal source have been performed. These measurements have the inherent problem that active measurements require a significantly larger dynamic range than passive ones. Since the receivers and detectors are designed for thermal input signals they are easily saturated by the much stronger active signal.

Concerning the optics of the active illumination system, different rectangular horn antennas have been considered. For images covering only a small elevation range a low gain rectangular horn (Figure 11) can be mounted on the azimuth platform of SPIRA. To cover images with a wider field of view a horn antenna with higher gain will be attached to rotating reflector of SPIRA in order to track the antenna pattern. The direct crosstalk between these feeds and the receiver has to be investigated. To minimize this effect, a low side lobe antenna, like corrugated feed horn, must be considered.

To illuminate the scene a coherent continuous wave (CW) signal or an incoherent broadband noise source can be used. In general the broadband noise will reduce interferences and thus the speckle noise in the image. However, even the relatively broad 2 GHz detection bandwidth of SPIRA cannot prevent speckles completely if a single noise source is used. This would require illuminating the scene with extended noise sources from different directions.

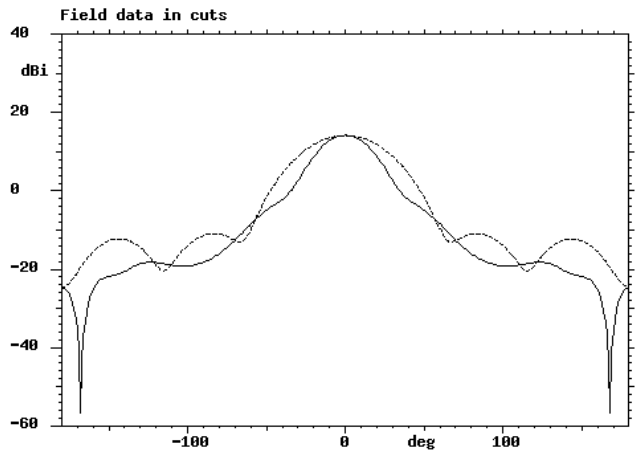

Figure 11: 91 GHz radiation pattern in H-plane (line) and E-plane (dotted) for the low-gain rectangular horn for active illumination.

A CW illumination produces much stronger speckle artifacts in the image, as shown in Figures 12. On the other hand it has the advantage that it will provide higher sensitivity and dynamic range, especially when used in combination with digital signal processing techniques. For this device an active W-band x6 multiplier chain, driven by a six times lower CW frequency from a synthesizer, has been chosen.

When the CW signal source is tuned outside of the 2-4 GHz IF bandwidth of the passive receiver, it can be still detected with separate narrow band detectors tuned to this external frequency, which would allow observing active and passive images simultaneously.

Moreover, in the experiments we conducted with active illumination, strong reflection from metal parts in front of the transmitting antenna, and increase scattering in received images were observed. However, these effects seem to be useful to better understand the shape of highly reflective metal parts. Considering the scene in Figure 13, where on the left a periodical metal structure constitutes the wall of a building and observing the images taken by SPIRA, the same periodical structure can be seen in Q and U images, while in passive image the wall appears flat.

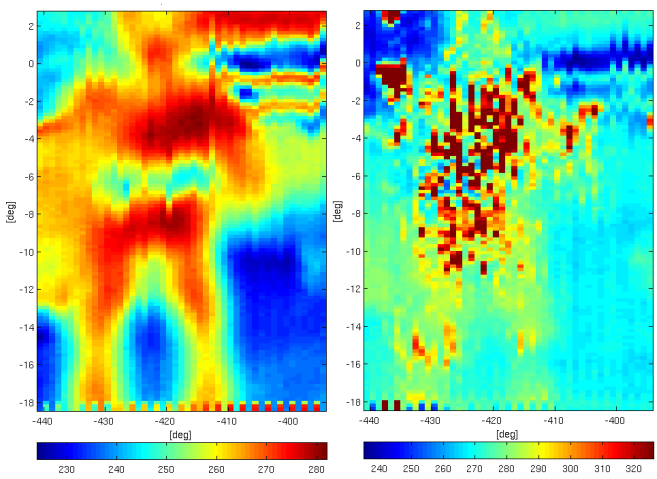

Figure 12: Passive (left) and active (right) images of a man hiding two metal plates behind his coat, taken by SPIRA. The speckle artifacts in the active image are significant.

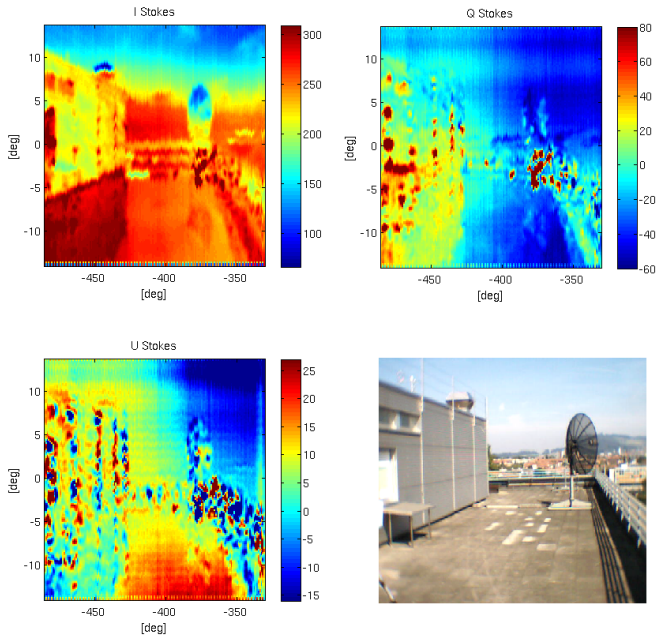

Figure 13: I, Q and U Stokes images of a scene (bottom right) taken by SPIRA, with active setup.

Further investigations on observation and modeling of periodical metal and dielectric structures will follow, as well as improvements in the active illumination equipment.

V. Conclusion

An overview of the activities of the microwave research group in Institute of Applied Physics of University of Bern is given. All the topics presented are still under continuous development and investigation. The results of our efforts look promising and further outcome will be presented in future.

Acknowledgements

The development work for this project has been funded by Armasuisse W+T under Project No. R-3210/040-11.

References

[1] A. Duric, A. Magun, A. Murk, C. Mätzler, N. Kämpfer: The Fully Polarimetric Imaging Radiometer SPIRA at 91 GHz, IEEE Transactions on Geoscience and Remote Sensing, vol.: 46, no.: 8, pp.: 2323-2336, 2008.

[2] C.Eiachi, J. Van Zyl: Introduction to the physics and techniques of Remote Sensing, 2nd Ed. Wiley.

[3] M. Canavero, A. Murk: Radiometric Modeling at 91 GHz, Research Report N° 2010-15-MW, IAP University of Bern, December 2010

[4] A. Duric, A. Magun: Polarimetric Measurements with a Fully Polarimetric Imaging Radiometer at 91 GHz, Proceedings of International Joint conference of 4th ESA workshop on Millimeter-Wave Technology and App.,Espoo, Finland, February 2006